A MODEL COMPOSITE ASSESSMENT OF THE ENHANCEMENT OF ARCTIC WARMING BY SEA ICE RETREAT

By

Colin P. Murray

RECOMMENDED:

Advisory Committee Chair

Chair, Atmospheric Sciences Program

APPROVED:

Dean, College of Natural Sciences and Mathematics

Dean of the Graduate School

April 17, 2006

Date

# A MODEL COMPOSITE ASSESSMENT OF THE ENHANCEMENT OF ARCTIC WARMING BY SEA ICE RETREAT

A

THESIS

Presented to the Faculty

of the University of Alaska Fairbanks

in Partial Fulfillment of the Requirements

for the Degree of

MASTER OF SCIENCE

By

Colin P. Murray, M.S.



Fairbanks, Alaska

May 2006

## Abstract

Five global climate models used in the Arctic Climate Impact Assessment are utilized to estimate the local enhancement of Arctic warming attributable to sea ice retreat in 21st century B2-scenario greenhouse gas (GHG) simulations. The models show a wide range of ice retreat, resulting in a corresponding range in the enhancement of warming. The enhancement is highly seasonal, varying *locally* from essentially zero in the summer to several degrees (˚C) in the late autumn and early winter. The composite climate model response to GHG forcing manifests as a nonlinear amplification of seasonally modulated warming enhancement. The magnitude of the warming enhancement increases with the threshold decline in ice concentration used to define retreat because higher thresholds better isolate the warming enhancement signal over ice retreat areas. A threshold of 20% ensures that all models in this study have enough ice retreat area to sample the enhancement because all start with ice concentrations at least that high over substantial northern hemisphere areas. All estimates are lower bounds because they do not account for advective effects.

# Table of Contents

Page

List of Figures

Page

List of Tables

Page

# Acknowledgements

I gratefully acknowledge the pivotal guidance and support of my major advisor Dr. John E. Walsh, UAF President's Professor of Global Change and Chief Scientist of the International Arctic Research Center. We jointly authored the paper (Murray and Walsh, 2005) from which this thesis is substantially drawn. His counsel was instrumental throughout the research project, and his suggestions for, and contribution to, the written manuscript were essential for its successful completion. I thank William Chapman from the Department of Atmospheric Sciences at the University of Illinois for data processing assistance essential for initiation of the project. Finally, I warmly thank my family and committee members for their support and the many teachers at UAF and elsewhere whose accumulated labors have allowed me the privilege of discerning some small measure of the beauty in the mathematical understructure of our reality. This work was supported by the National Science Foundation's Cooperative Agreement (OPP-0327664) with the International Arctic Research Center.

## 1. Introduction

Global climate models have consistently indicated a polar amplification of greenhouse-driven warming, dating back to the earliest global model experiments of the 1970s (Manabe and Wetherald, 1975) and continuing through the recent decade (e.g., ACIA, 2004). A snow/ice albedo-temperature feedback triggered by an initial warming is among the factors that can contribute to a polar amplification of the near-surface warming. The decrease of surface albedo from 0.6-0.8 over snow-covered land or sea ice, to 0.1-0.3 over open ocean or bare land, will give strong leverage to an initial warming (or cooling) near the snow/ice margin, especially during spring and summer when insolation is strongest. See Figure 1 for a simple diagram. Land and ocean areas that lose snow and ice cover undergo a major adjustment in their surface radiation balance: increased radiative absorption and emission, as well as a large increase of the sensible heat flux to overlying cold air. This suggests that an externally forced (e.g., greenhouse-gas driven) warming should be greatest over areas in which snow and ice disappear during the course of a climate change.

The 21$^{st}$-century reduction of sea ice is substantial in most greenhouse-driven simulations of climate by global models, and the retreat of sea ice is known to play a substantial role in their globally-averaged warming response, e.g., Rind et al. (1995). Visualizations of climate simulations used in the Arctic Climate Impact Assessment (ACIA, 2004) show striking coherence of surface air temperature warming patterns over marginal ice zones. An example is shown in Figure 2. This suggests that direct enhancement of Arctic warming by sea ice retreat may be quantifiable in terms of the

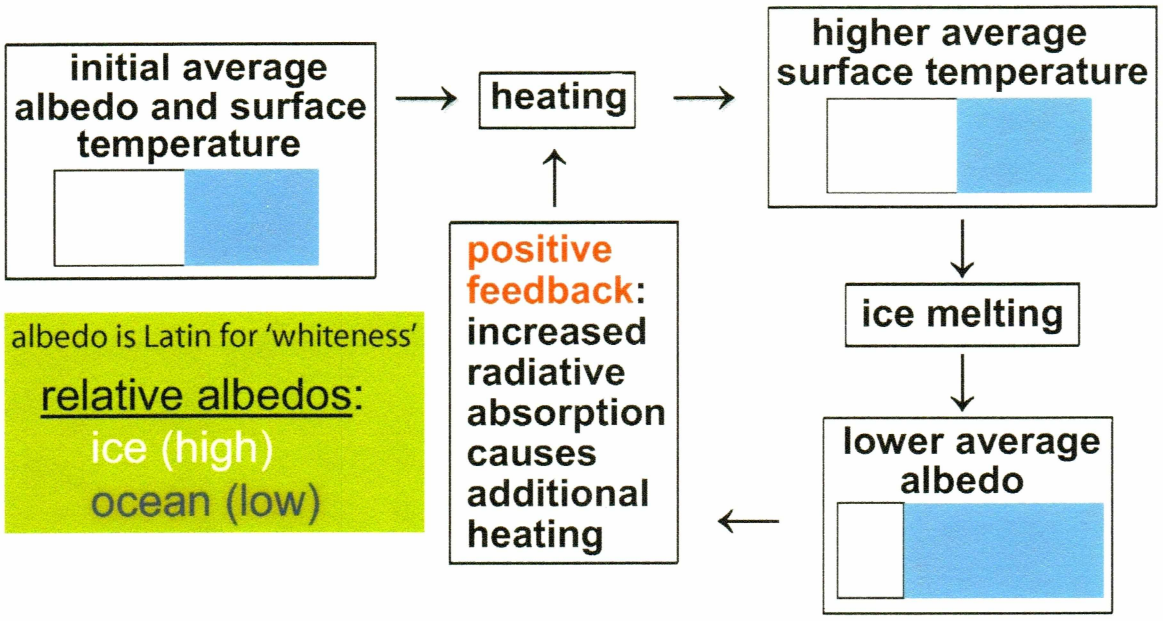


Figure 1. Snow/ice albedo-temperature (positive) feedback.

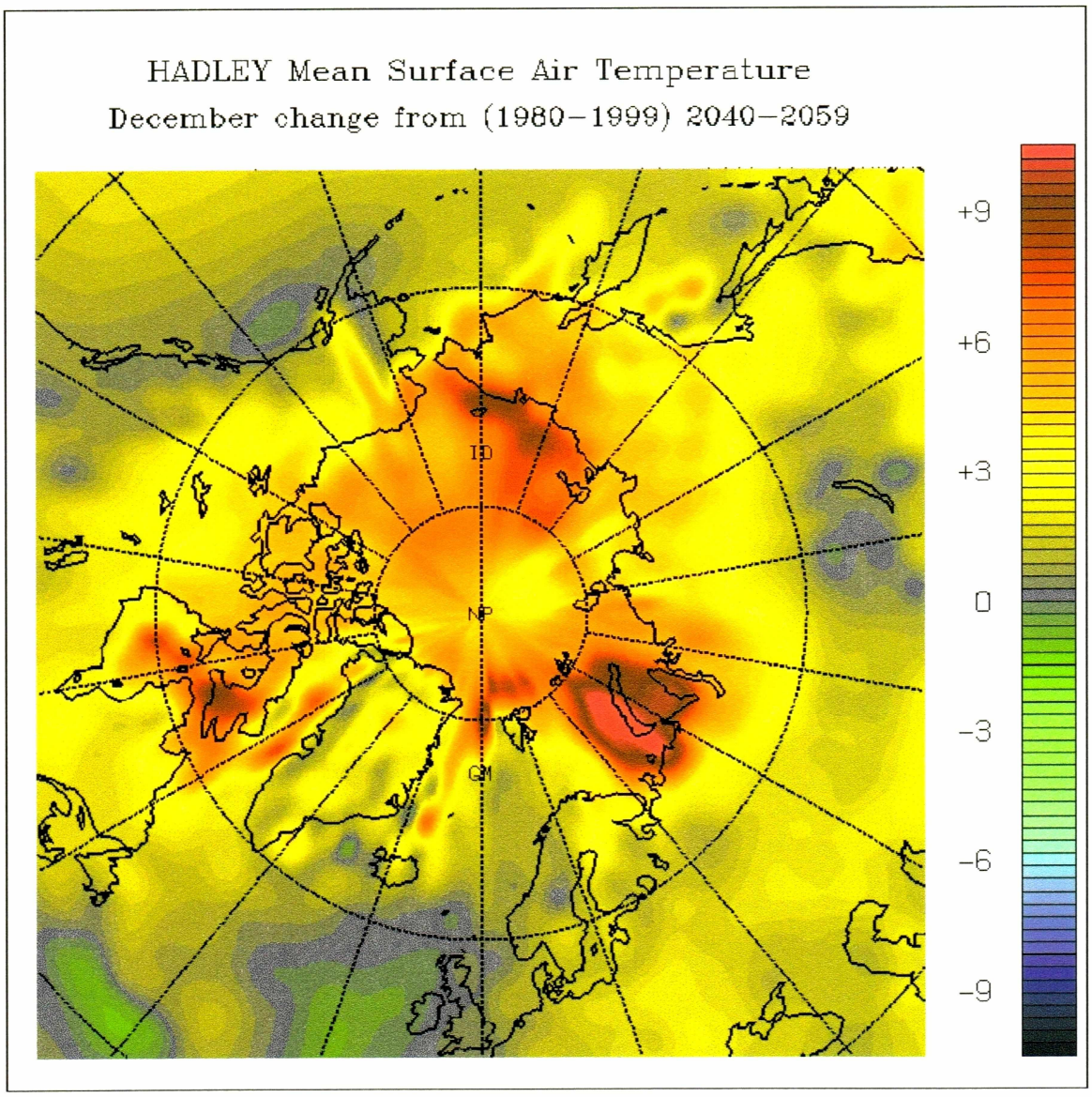


Figure 2. Coherent warming patterns over marginal ice zones from the HadCM3 climate model (Hadley Centre for Climate Prediction and Research, United Kingdom)

difference between the warming of surface air temperatures over northern hemisphere areas of sea ice retreat and the warming over proximate areas. Insofar as such a differential warming is bound to be diluted by advection of heat gained from newly open water, and perhaps from other atmospheric processes, it represents a lower bound on the enhancement of warming by sea ice retreat. This constraint is illustrated in Figure 3. Nevertheless, these lower bound estimates may serve as a starting point for quantitative assessments of the net contribution of local sea ice feedbacks to the polar amplification of greenhouse warming, and its calculation and analysis is the goal of this paper.

## 2. Models

Surface air temperature observations in the Arctic over the last century show a statistically significant warming trend (Figure 4). Concern over the impact of Arctic warming on human systems led to the formation of the Arctic Climate Impact Assessment (ACIA, 2004), an international project "to assess current knowledge of Arctic climate variability and change, and its consequences through the 21$^{st}$ century". ACIA used five global climate models to explore how the Arctic will respond to increasing greenhouse gas concentrations over the next century. The models and details of their configurations are listed in Table 1. They are all well documented in the published literature and were run to the year 2100 using the moderate B2 greenhouse gas emissions scenario (IPCC, 2000), which assumes medium growth (relative to the IPCC's other five harmonized climate change scenarios) in global population, GDP, energy use, etc. The six scenarios span a range of possible paths of economic and social change over

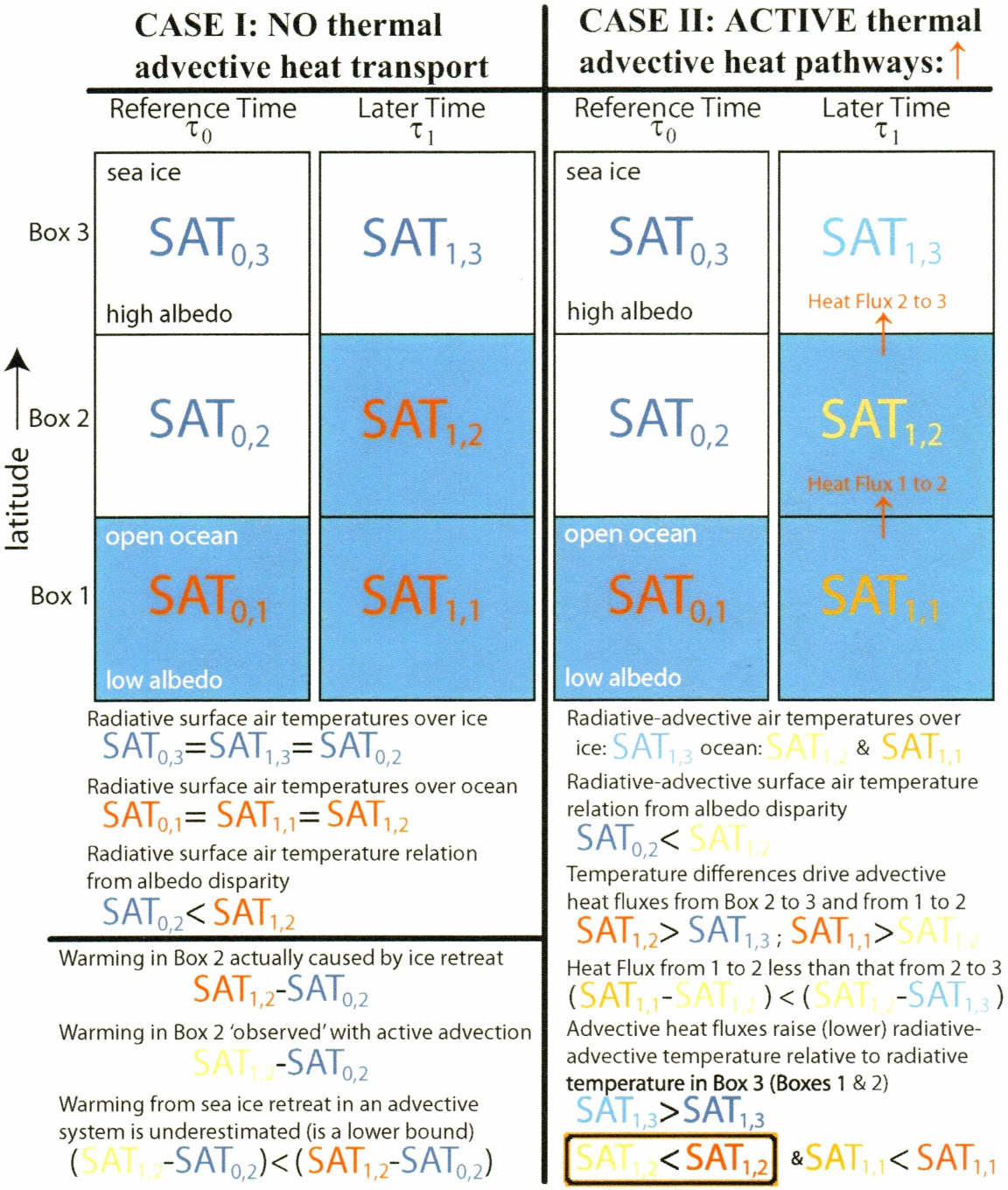


Figure 3. An idealized conceptual model of the effect of thermal advective leakage on surface air temperatures (SAT's) in ice retreat areas. Define a closed ice margin system to comprise three contiguous areal boxes receiving spatially homogeneous and time-invariant insolation. Box 1 is open ocean, and Boxes 2 and 3 are covered with sea ice at reference time $\tau_0$.Ocean water absorbs more solar radiation (and emits more longwave

thermal radiation) than sea ice, heating surface air over a patch of ocean more than it would have been heated by the same insolation had the patch of ocean been covered by sea ice. Box 1 therefore has a higher surface air temperature than Boxes 2 and 3 at time $\tau_0$. Let Box 2 undergo complete sea ice retreat during a time interval that starts at $\tau_0$ and ends at time $\tau_1$. Cases I and II show SAT response to ice retreat in Box 2 for radiative and radiative-advective systems ice margin systems, i.e. without and with heat advection between boxes. Case I quantifies the warming attributable to sea ice retreat in Box 2. Case II illustrates that Box 2 loses more heat energy from advection than it gains. Therefore warming in Box 2 of an advective system will always underestimate the warming due to sea ice retreat because some of the increase in heat energy is lost to advection.

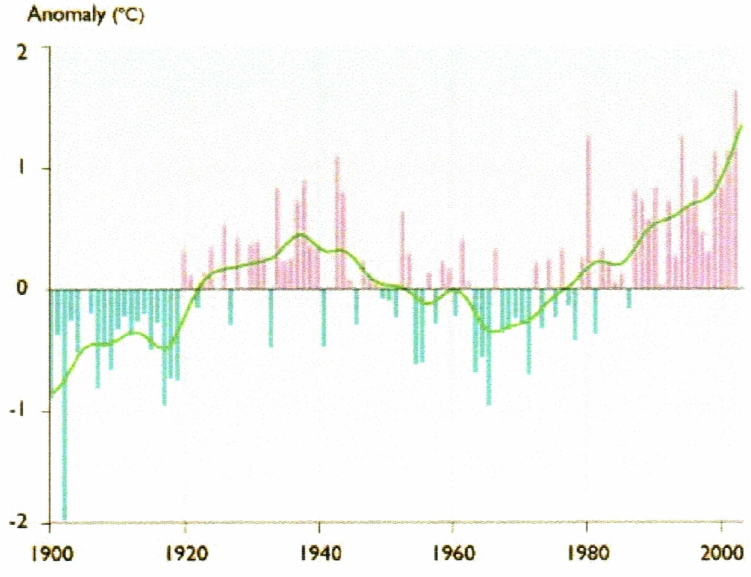


Figure 4. Annual anomalies of land-surface air temperature in the Arctic (60° to 90° N) for the period 1900 to 2003 using the GHCN dataset (updated from Peterson and Vose, 1997). Anomalies are calculated relative to the 1961–1990 average. The smoothed curve was created using a 21-point binomial filter, which approximates a 10-year running mean. (Figure 2.6 from ACIA, 2005)

Table 1. The five global climate models (Table 4.1 from ACIA, 2005)

| | Atmospheric resolution[a] | Ocean resolution[b] | Land-surface scheme[c] | Sea-ice model[d] | Flux adjustment[e] | Primary reference |
|---|---|---|---|---|---|---|
| CGCM2 | | | | | | |
| Canadian Centre for Climate Modelling and Analysis, Canada | T32 (3.8° x 3.8°) L10 | 1.8° x 1.8° L29 | M, BB, F, R | T, R | H, W | Flato and Boer, 2001 |
| CSM_1.4 | | | | | | |
| National Center for Atmospheric Research, United States | T42 (2.8° x 2.8°) L18 | 2.0° x 2.4° L45 | C, F | T, R | - | Boville et al., 2001 |
| ECHAM4/OPYC3 | | | | | | |
| Max-Planck Institute for Meteorology, Germany | T42 (2.8° x 2.8°) L19 | 2.8° x 2.8° L11 | M, BB, R | T, R | H*, W* | Roeckner et al., 1996 |
| GFDL-R30_c | | | | | | |
| Geophysical Fluid Dynamics Laboratory, United States | R30 (2.25° x 3.75°) L14 | 2.25° x 1.875° L18 | B, R | T, F | H, W | Delworth et al., 2002 |
| HadCM3 | | | | | | |
| Hadley Centre for Climate Prediction and Research, United Kingdom | 2.5° x 3.75° L19 | 1.25° x 1.25° L20 | C, F, R | T, F | - | Gordon et al., 2000 |

[a]Horizontal resolution is expressed either as degrees latitude by longitude or as a spectral truncation (either triangular (T) or rhomboidal (R)) with a rough translation to degrees latitude and longitude. Vertical resolution (L) is the number of vertical levels; [b]Horizontal resolution is expressed as degrees latitude by longitude, while vertical resolution (L) is the number of vertical levels; [c]B=standard bucket hydrology scheme (single-layer reservoir of soil moisture which changes with the combined action of precipitation (snowmelt) and evaporation, and produces runoff when the water content reaches the prescribed maximum value); BB=modified bucket scheme with spatially varying soil moisture capacity and/or surface resistance; M=multilayer temperature scheme; C=complex land-surface scheme usually including multiple soil layers for temperature and moisture, and an explicit representation of canopy processes; F=soil freezing processes included; R=river routing of the discharge to the ocean (land surface is represented as a set of river drainage basins); [d]T=thermodynamic ice model; F="free drift" dynamics; R=ice rheology included; [e]H=heat flux; W=freshwater flux; asterisks indicate annual mean flux adjustment only.

the 21st century, and estimate greenhouse gas emissions from their associated land use, industrial activity, etc. Figure 5 shows projected anthropogenic emissions of carbon dioxide, nitrous oxide, methane, and sulfur for all six IPCC scenarios.

$CO_2$ concentrations in all simulations vary with time according to observationally-derived values (e.g. Figure 6) during a spin-up covering at least the latter portion of the 20th century that culminates in a concentration of 370 ppm in the year 2000, and to the B2 scenario thereafter to the end of the 21st century where it reaches approximately 600 ppm. Thus, each model begins its B2-prescribed $CO_2$ forcing at the start of 2000, with 'effective' initial conditions for each being that model's simulated climate (including sea ice) for that time. The Canadian Global Climate Model (CGCM2) results are actually averages over three members of an ensemble of simulations that differed only by slight perturbations of the initial conditions. The three ensemble members evolved much more similarly to each other than to the simulations by the other models. The ACIA models are consistent in projecting polar amplification of global warming and contraction of northern hemisphere sea ice extent over the 21st century. (Figure 7)

All five climate models are fully coupled atmosphere-land-ocean-sea ice models, where each constituent model (e.g. atmosphere) interacts over time by exchanging boundary condition information with at least one other constituent model (e.g. sea ice interacts with both atmosphere and ocean). However, each of the five climate models implements its constituent models, and the way information is exchanged between them (coupling), in a different way. See Table 1 for details. This diversity in model construction allows evaluation of the sensitivity of climate forecast solutions

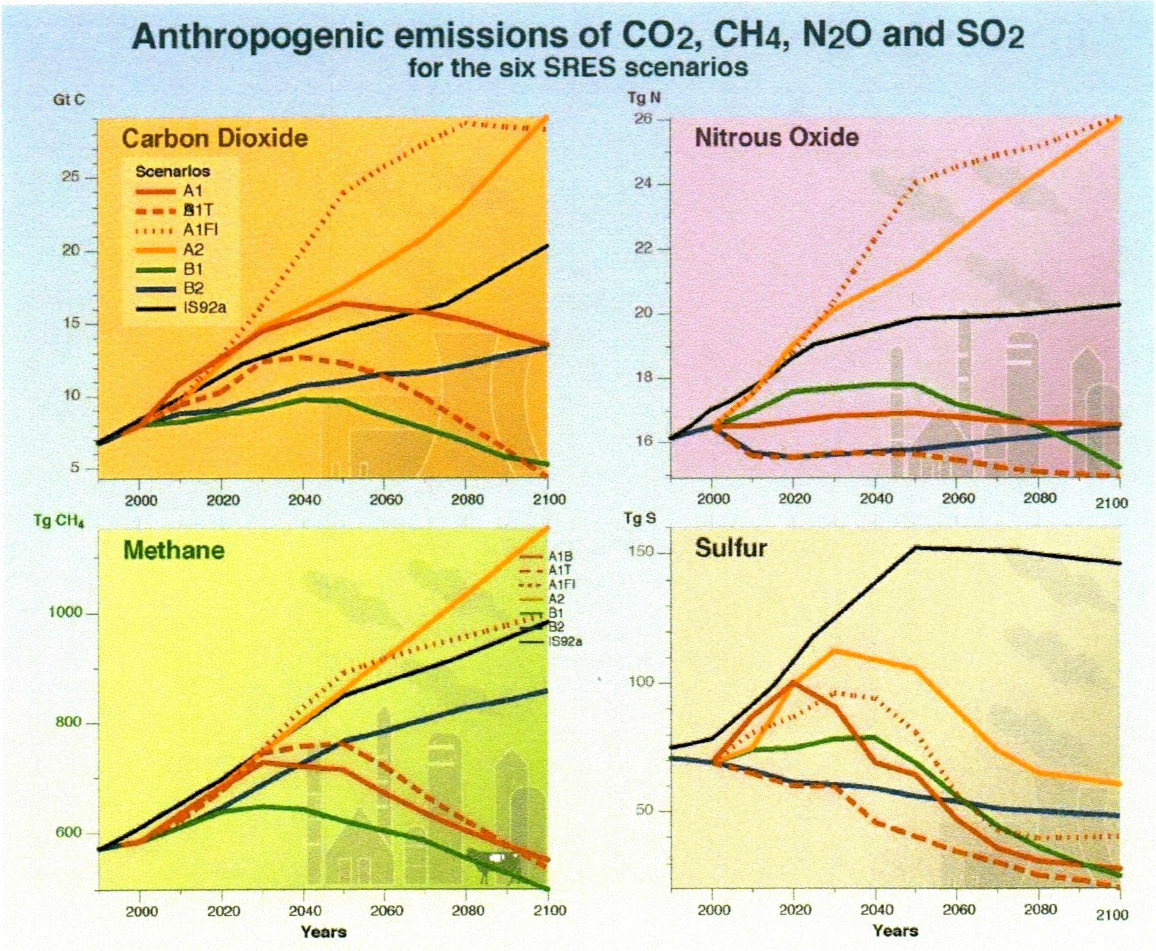


Figure 5. Anthropogenic greenhouse gas emissions for the six Intergovernmental Panel on Climate Change (IPCC) climate change scenarios (from IPCC, 2001). Note that B2 scenario projections for each gas lie close to the median of all six scenarios.

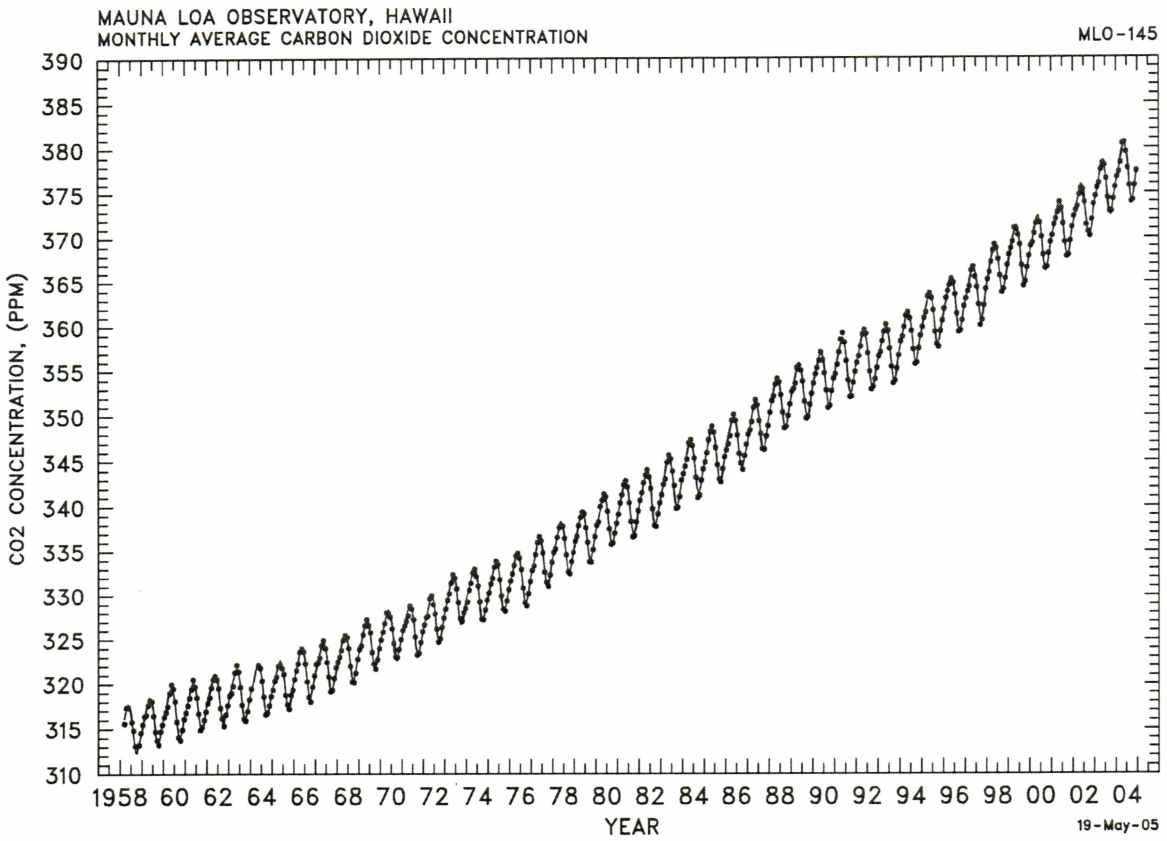


Figure 6. Monthly average carbon dioxide concentrations from data measured at the Mauna Loa Observatory, Hawaii. Seasonal variation associated with biospheric uptake and release is superimposed upon a clearly non-linear growth trend. (from Keeling and Whorf, 2005.)

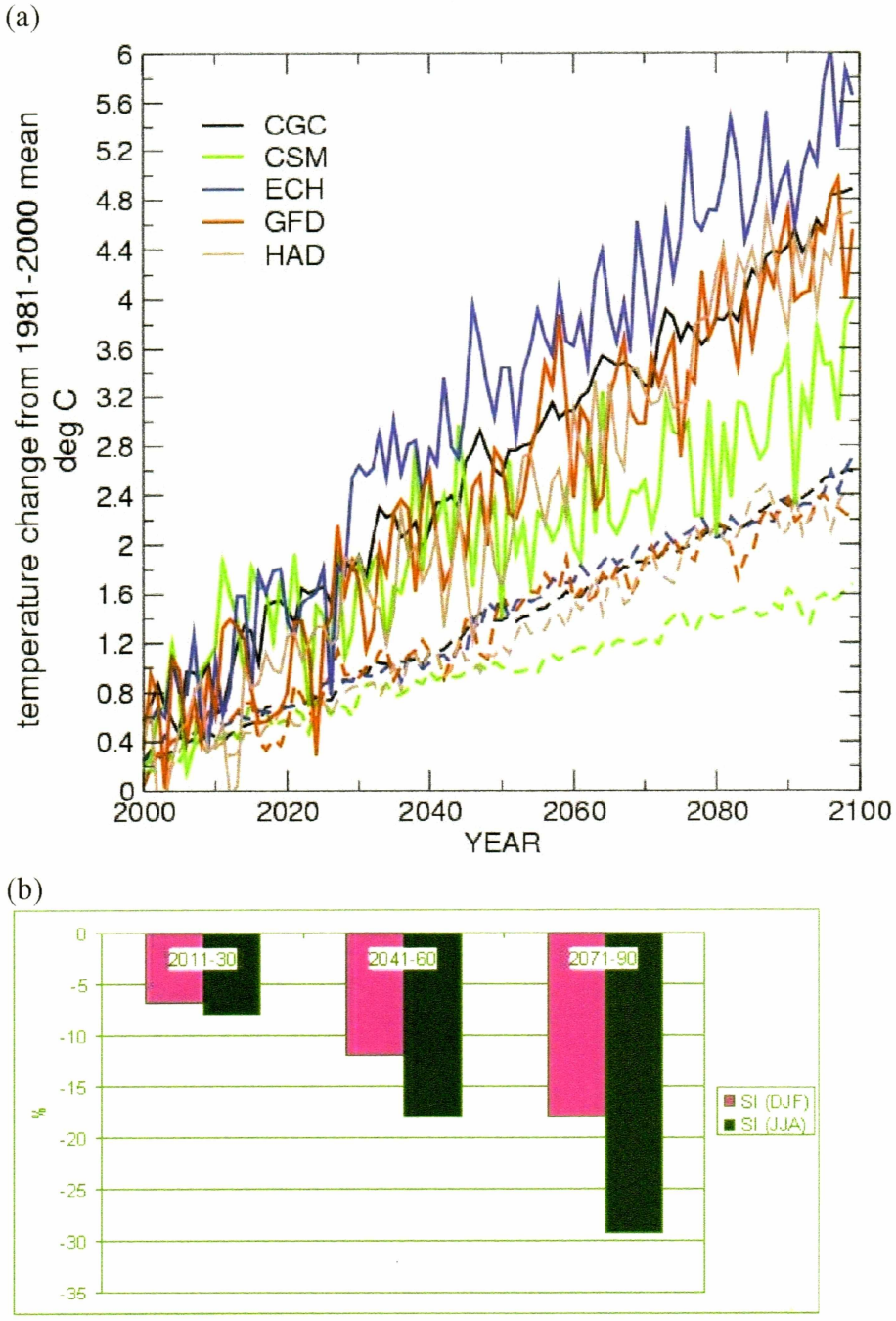


Figure 7. ACIA B-2 scenario climate model results. (a) Changes in annual mean surface air temperature relative to the baseline period 1981-2000. Dashed lines are averages over the NH and solid lines are averages over the Arctic (b) Model composite winter and summer decreases in sea ice extent relative to the baseline period 1981-2000 for periods 2011-2030, 2041-2060, and 2071-2090

(for a given forcing, e.g. B2) to mathematical and physical assumptions implicit in the model construction, and is the fundamental prerequisite for a model composite assessment. The sea ice models are particularly important. All are 'thermodynamic', which means that they are free to respond thermodynamically and dynamically to atmospheric and oceanic forcing. However, they differ in dynamical formulation, e.g., in their ice rheologies.

## 3. Methodology

The 'raw' data for this numerical experiment consists of time series of monthly-average records from 1990 to 2100 of two-dimensional surface air temperature (hereafter denoted as "air temperature") and sea ice concentration fields from all five ACIA models mapped onto a common global 2.5° grid. The grid cells consist of rhomboidal areal elements that undergo a poleward decline in area, and two circular discs at the poles, each symmetric with the axis of rotation. The air temperature and sea ice concentration fields are processed to obtain monthly time series of differential temperature anomaly (*DTA*), which are differences between air temperature changes from the models' present-day (1990-2000) climatologies area-averaged over regions of sea ice retreat and over proximate ice-free areas. Calculation of *DTA* is made on a calendar-month basis for each of the five models. The first step for each model and calendar month is to create air temperature and ice concentration anomaly time series spanning the 2001-2100 period. See Figure 8 for a representative illustration. Hereafter these are denoted by *TA* for temperature anomaly and *ICR* for ice concentration reduction. *TA* is calculated by

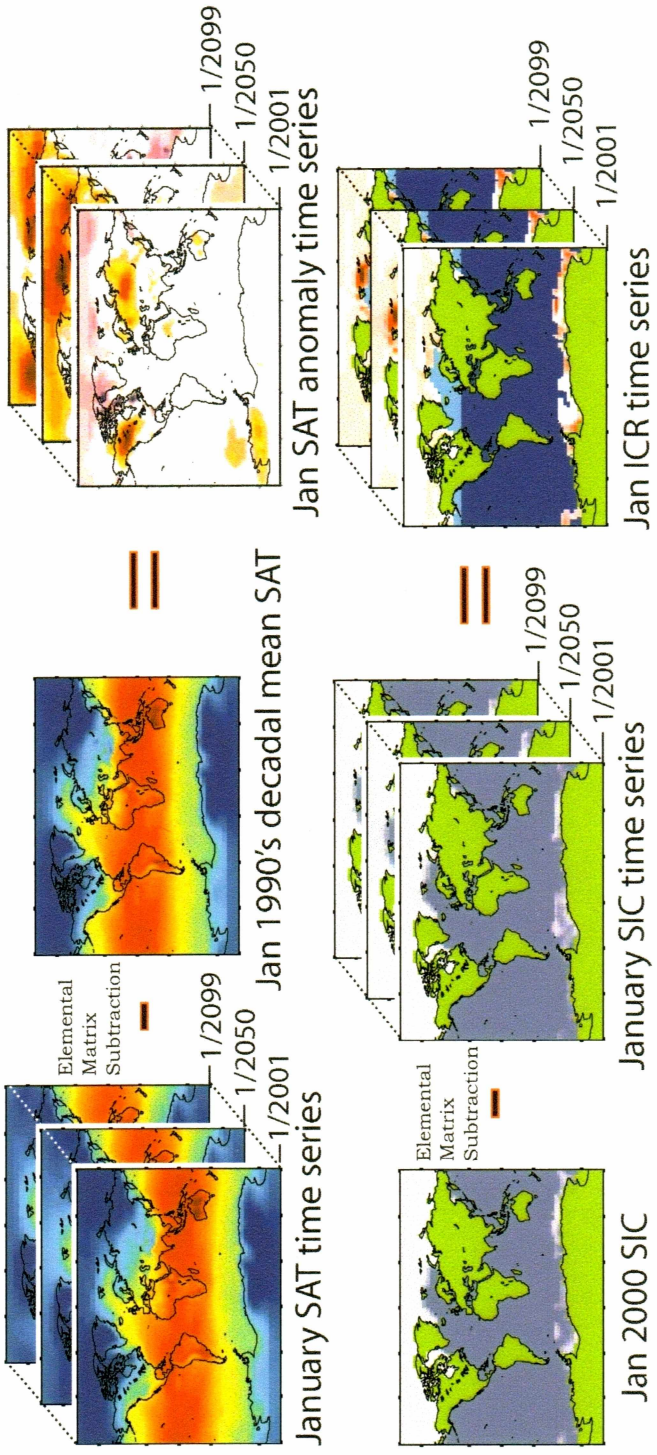


Figure 8. Illustration of surface air temperature and ice concentration anomaly time series calculation for calendar-month January for the ECHAM4/OPYC3 model. Elemental matrix subtraction is an operation between operands of the same size where entries of similar position are differenced.

elemental (two-dimensional) matrix subtraction: each record in a surface air temperature time series less its 1990's decadal mean surface air temperature. *ICR* is a percent difference in ice concentrations and is also calculated by elemental (two-dimensional) matrix subtraction: each record in an ice concentration time series is subtracted from its year-2000 record, such that positive values indicate a decrease in ice concentration from the year 2000. Ice concentration is calculated with respect to complete coverage (unity or 100%), and therefore so is *ICR*. A grid point with an *ICR* value of 0.2 has undergone a reduction of sea ice coverage equal to 20% of maximum possible (complete) coverage, not a 20% reduction with respect to the initial year 2000 coverage. A grid point is considered to have undergone retreat when its *ICR* value exceeds an arbitrary threshold (hereafter referred to as "retreat threshold"). Higher retreat thresholds delimit less area of ice-retreat for inclusion in the calculations because they require greater decreases in ice concentration in order for grid points to be considered to have undergone sea ice retreat.

The next step for each model and calendar-month is the synthesis of *TA* and *ICR* data to create scalar time series of area-averaged temperature anomalies. Each two-dimensional record in the *ICR* time series is used to construct a "mask" for area-weighted averaging of its contemporaneous two-dimensional record in the *TA* time series. Figure 9 shows the January 2050 records of *TA* and *ICR* for the ECHAM4 model. Masks delimit ice-retreat area over which to average *TA* by selecting those grid cells for which the difference in concentration is greater than some retreat threshold. Area-weighted averages of *TA* calculated over Northern Hemisphere (NH) regions of sea ice retreat will hereafter be denoted by $\overline{TA}_{retreat}$, and the regions over which they are averaged

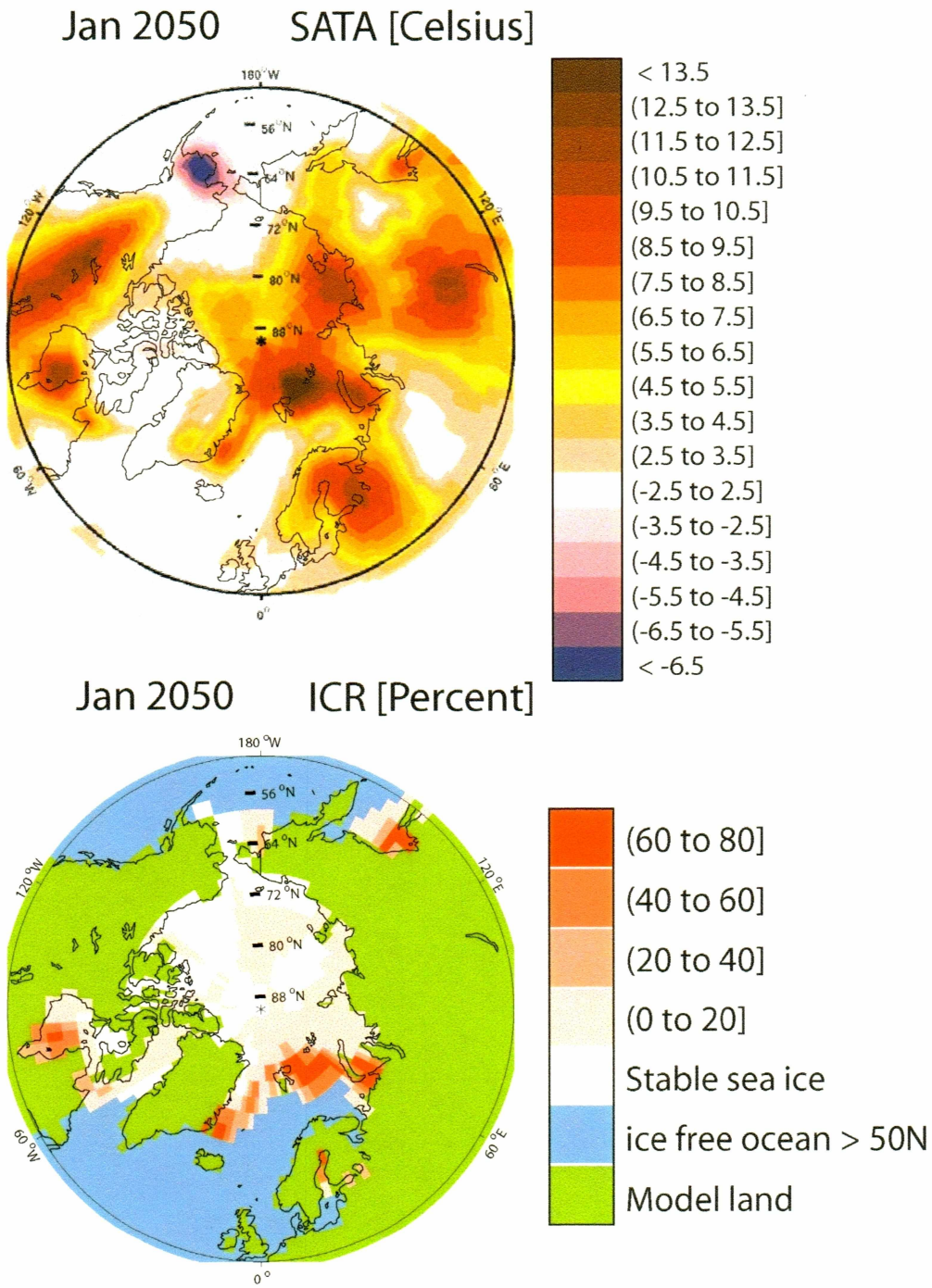


Figure 9. Illustration of the ECHAM4/OPYC3 model's calendar-month January surface air temperature and ice concentration anomaly records for year 2050. Note the spatial co-location of the warming and ice concentration reduction anomalies.

will be referred to as "ice-retreat". The Figure 9 *ICR* plot shows strong ice retreat in the Barents Sea, Sea of Okhotsk, and Hudson Bay. A high retreat threshold (e.g. 50%) will have an ice-retreat area comprising only these three regions (only the darkest red). A lower threshold (e.g. 20%) will have a much larger ice-retreat area (all shades of red in the *ICR* plot). Note that the contemporaneous *TA* field has local maxima coincident with *ICR* local maxima. If $\overline{TA}_{retreat}$ values evaluated over ice-retreat regions are in any way influenced by the retreat of sea ice, then they will be dependent upon retreat threshold, i.e., greater average retreat over the averaging region means greater influence from the process of ice retreat on the area-averaged air temperature anomaly. It is important to assess the functional sensitivity of $\overline{TA}_{retreat}$ to variation in retreat threshold. Therefore, we calculate 101 separate $\overline{TA}_{retreat}$ time series by area-weighted averaging the *TA* time series over 101 different NH ice-retreat regions delimited by successive application of the monotonically-increasing thresholds $ICR > 0\%$, $\geq 1\%$, $\geq 2\%$, …, $\geq 98\%$, $\geq 99\%$, and $= 100\%$.

A "reference" scalar air temperature anomaly time series is constructed by area-weighted averaging *TA* over oceanic regions poleward of 50°N that are ice-free ocean in that model-month's year-2000 ice concentration field. The example in the Figure 9 *ICR* plot delineates this area in turquoise. This scalar air temperature anomaly time series will hereafter be denoted by $\overline{TA}_{no-ice}$, and the region over which it is averaged will be referred to as "ice-free". Note that it is not dependent upon retreat threshold.

The final step for each model-month entails calculation of 101 *DTA* scalar time series by subtraction of contemporaneous elements of the $\overline{TA}_{no-ice}$ time series from each of the 101 $\overline{TA}_{retreat}$ time series. Note that this means that *DTA* can vary with retreat threshold. Processing all model-months yields 60 *DTA* data sets (12 months x 5 models), each set comprised of 101 monthly-average *DTA* time series that functionally depend on time ($\tau$) and retreat-threshold (*RT*), i.e.

$$DTA(\tau, RT) = \overline{TA}_{retreat}(\tau, RT) - \overline{TA}_{no-ice}(\tau).$$

## 4. Results and Analysis

The entire November calendar-month GFDL_R30_c data set is plotted in Figure 10 to illustrate differential temperature anomaly (*DTA*) sensitivity to retreat threshold. Retreat threshold lies along the abscissa, and its 101 *DTA* time series are displayed in retreat-threshold order, each forming a column with contemporaneous elements horizontally synchronized. Note that the area of averaging decreases as the retreat threshold increases. The black region at high retreat thresholds indicates where the thresholds were so high that there was no area over which to average temperature anomaly. The ubiquity of *DTA* growth with retreat threshold throughout the record affirms the role of sea ice retreat in warming enhancement occurring over ice-retreat regions for this model-month. Although this example is typical of NH winter patterns in all the models, the strength of the correlation does vary seasonally. Nevertheless, we can state unequivocally that when and where sea ice retreat enhances warming, the magnitude of the warming generally increases with retreat threshold.

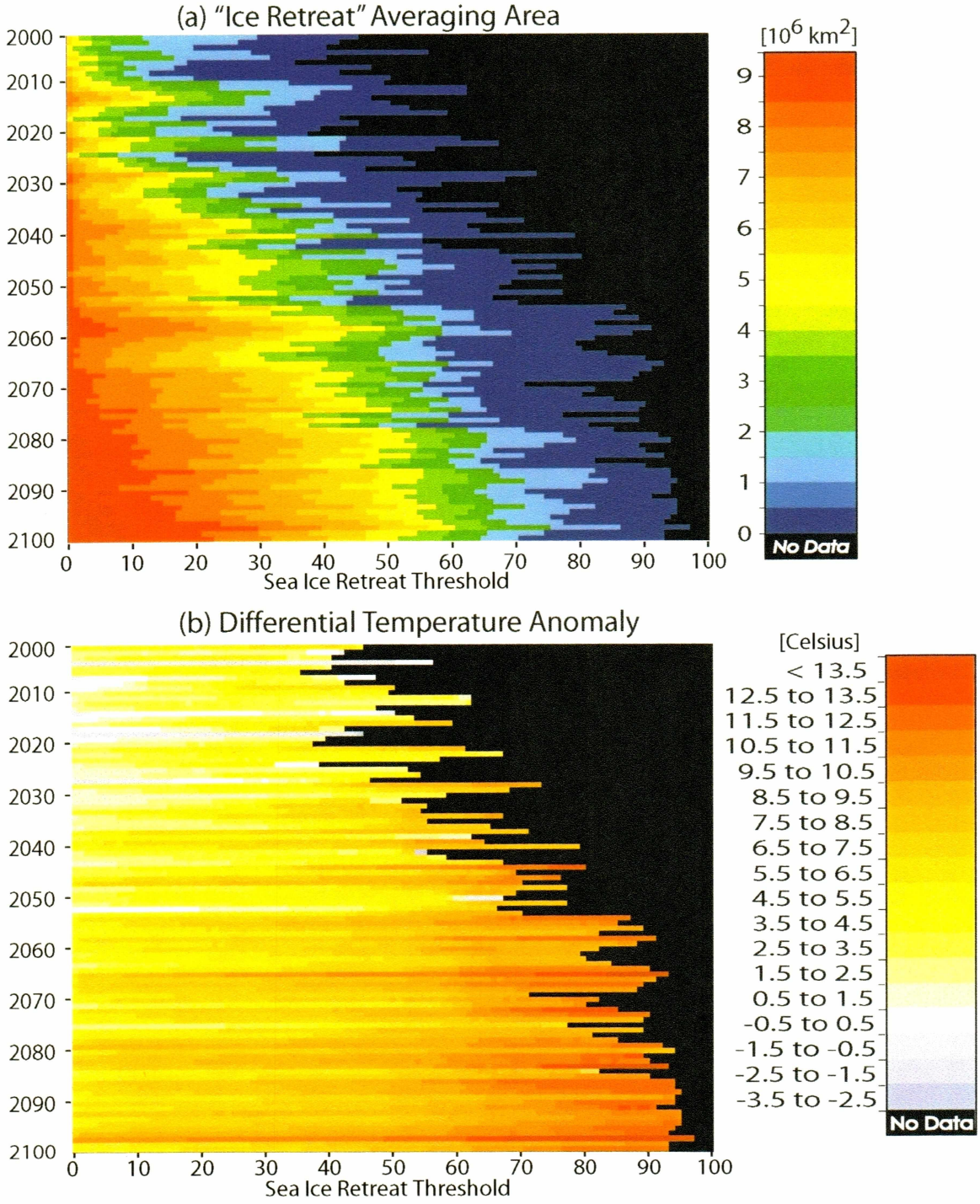


Figure 10. Differential Temperature Anomalies and corresponding ice retreat averaging area for GFDL_R30_c calendar-month November. Positive values indicate differential warming while negative values (pale blue) indicate differential cooling. The latter quantity indicates that SAT's warmed less over ice-retreat areas than over ice-free areas.

All calendar-monthly *DTA* time series with ice concentration reductions of at least 20% are collated for each model as "seasonal" plots, so that each successive vertical column of data in these plots is a *DTA* time series (extracted from a plot similar to Figure 10) for successive calendar months. This threshold is chosen for illustration because all models experienced concentrations of at least 20% over substantial areas, while the areas of (for example) 50% and 80% ice retreat were small in the early decades for some of the models. The seasonal *DTA* plots for all five models are shown in Figure 11. All five models show a seasonal modulation of *DTA*, i.e., they sustain a seasonal cycle of warming enhancement with substantive warming by sea ice retreat (of ice-retreat areas relative to ice-free areas) during winter and either negligible warming or slight cooling during summer. This signal occurs throughout the *DTA* data, including the earliest years of the 21$^{st}$ century when $CO_2$ concentration was still close to its year 2000 value, due to sea ice retreat associated with interannual variation in the position of the polar ice edge (with respect to the reference fields). Therefore the first several years of the *DTA* data may perhaps be viewed as being representative of a seasonally modulated signal in quasi-dynamic equilibrium, i.e. not undergoing systematic changes other than from the seasonal cycle, prior to response to the B2-scenario greenhouse gas forcing.

The time dependent response (inclusive of all feedback mechanisms) of the CGCM2 model manifests as a nonlinear (with respect to the seasonal cycle) amplification of warming enhancement that is most intense during late autumn and early winter. Contrarily, the CSM_1.4 model has no discernable centurial trend. The other three models' responses lie somewhere in between, with clearly defined warming enhancement

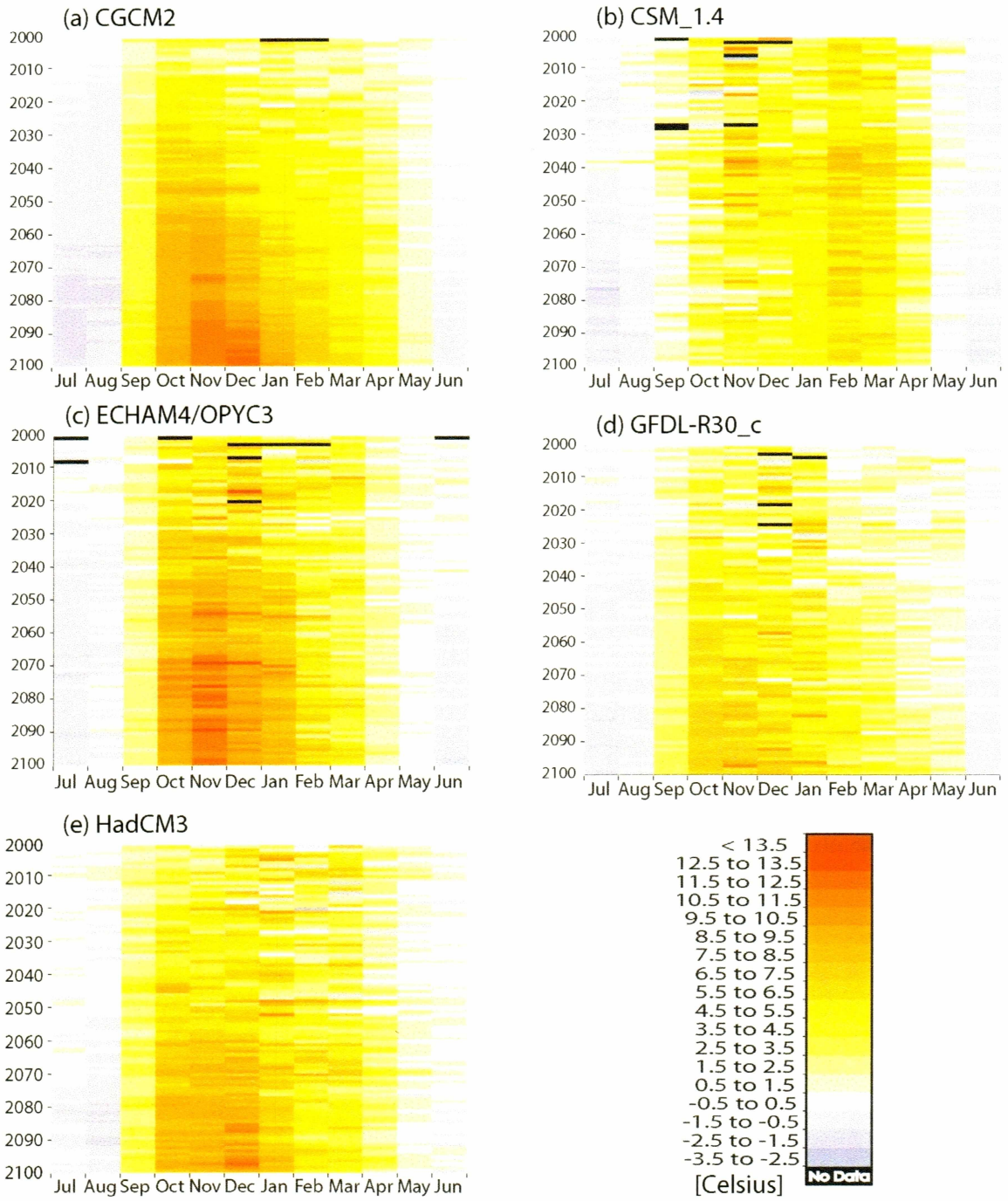


Figure 11. Calendar-month collation of *DTA* time series with ice retreat area calculated using a 20% retreat threshold. All models show a seasonal cycle of differential warming in winter and differential cooling in summer. Four show a non-linear amplification of this cycle over the 21st century: strong intensification of warming enhancement in winter and weak intensification of cooling enhancement in summer. The latter indicates that SAT's warmed less over ice-retreat areas than over ice-free areas (but still warmed).

increasing over time similar to that of the CGCM2 model, but with smaller magnitudes and modest phase differences. The CGCM2 and CSM_1.4 are thus the models most and least responsive to warming enhancement by sea ice retreat. The CGCM2 model started the B2 portion of the run with too little sea ice, and the CSM_1.4 model with too much, with respect to validated satellite observations of sea ice extent made during the early years of the 21$^{st}$ century. The CGCM2 model then proceeded incurring the most sea ice retreat of any of the models, and CSM_1.4 the least, through to the end of the runs in 2100. One explanation for the growth in warming enhancement experienced by the four models with the greatest sea ice retreat is that average ice concentration in the retreat region decreases with time, transforming the local surface radiative regime to increase surface air temperatures. The data in Figure 11 can be distilled by considering only the 2090's decadal mean of *DTA* (the average of the last 10 values on the y-axis), and by averaging over three-month seasons. Recall that air temperature anomalies are with respect to the 1990's decadal mean, therefore the 2090's decadal mean of *DTA* represents centurial warming. Figure 12 contains bar plots which show these values for each model, and their corresponding 2090's decadal mean of ice retreat area. We conclude that the wide range of sea ice retreat observed in the ACIA models directly corresponds with a wide range of warming enhancement by sea ice retreat.

Composite averages of model results tend to provide more realistic estimates than those from any single model, and a composite 'calendar-monthly' composite can be calculated by simple averaging of the 20% retreat threshold *DTA* data from all five models, i.e., those in Figure 11. However, the regularity of the composite seasonal cycle

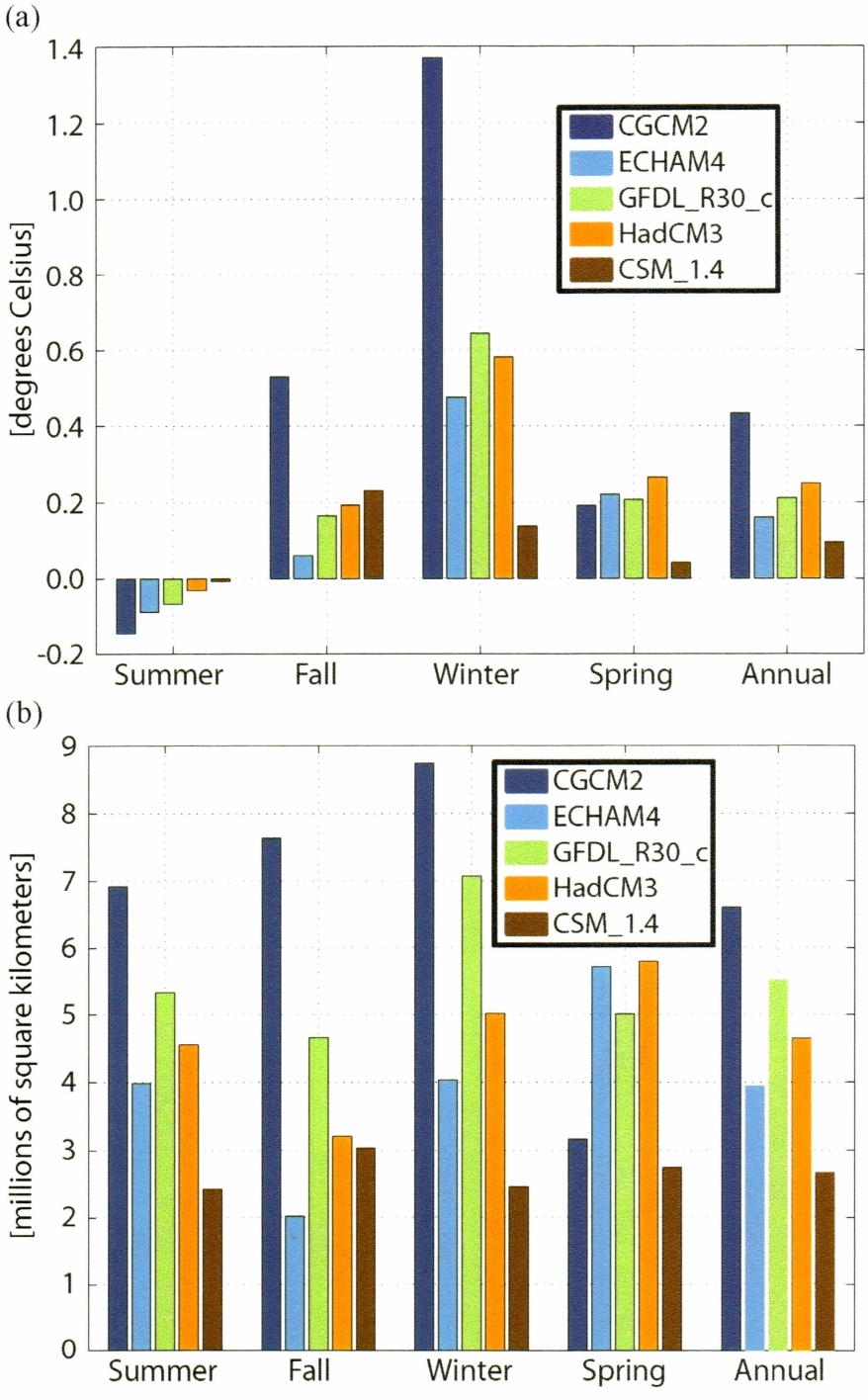


Figure 12. Relation between *DTA* and area of sea ice retreat amongst the five models: seasonal averages (over calendar-months) calculated with a 20% retreat threshold. (a) 2090's decadal mean Differential Temperature Anomaly (b) corresponding area of sea ice retreat during 2090's relative to year 2000

and its amplification over time is similar to that of the CGCM2 model. More can be learned by comparison of the relative magnitudes of the two components of composite *DTA*: composite $\overline{TA}_{retreat}$ and composite $\overline{TA}_{no-ice}$, so seasonal averages of the 2090's decadal mean of both are displayed in Figure 13. The areas over which averaging was performed to obtain the values in Figure 13 are regions of sea ice retreat from 2000 at a 20% retreat threshold (blue bars) and oceanic regions poleward of 50° N that were free of sea ice in 2000 (red bars). Surface air temperatures show increases in both regions during all seasons. The increases are larger during fall, winter, and spring, and very slightly less during summer, over areas of sea ice retreat than over ice-free areas. The winter maxima and summer minima signify the seasonality of warming, with that over ice retreat areas being much more pronounced. The warming over ice-free areas may be due at least in part to advective leakage of heat from ice-retreat areas. Both winter warming enhancement and the slight summer cooling are consistent with the ice insulation effect, which would be one aspect of changes in local surface radiation balance from sea ice retreat. We note that near-surface air temperatures generally exceed ocean surface temperatures during summer. The experiment design ensures that ice retreat (inclusive of all possible feedbacks and processes) is a leading reason for differences between the areas, and warming over ice-retreat areas is by definition local. Therefore we conclude that enhancement of warming by sea ice retreat is highly seasonal, varying *locally* from essentially zero in the summer to several degrees (°C) in the late autumn and early winter.

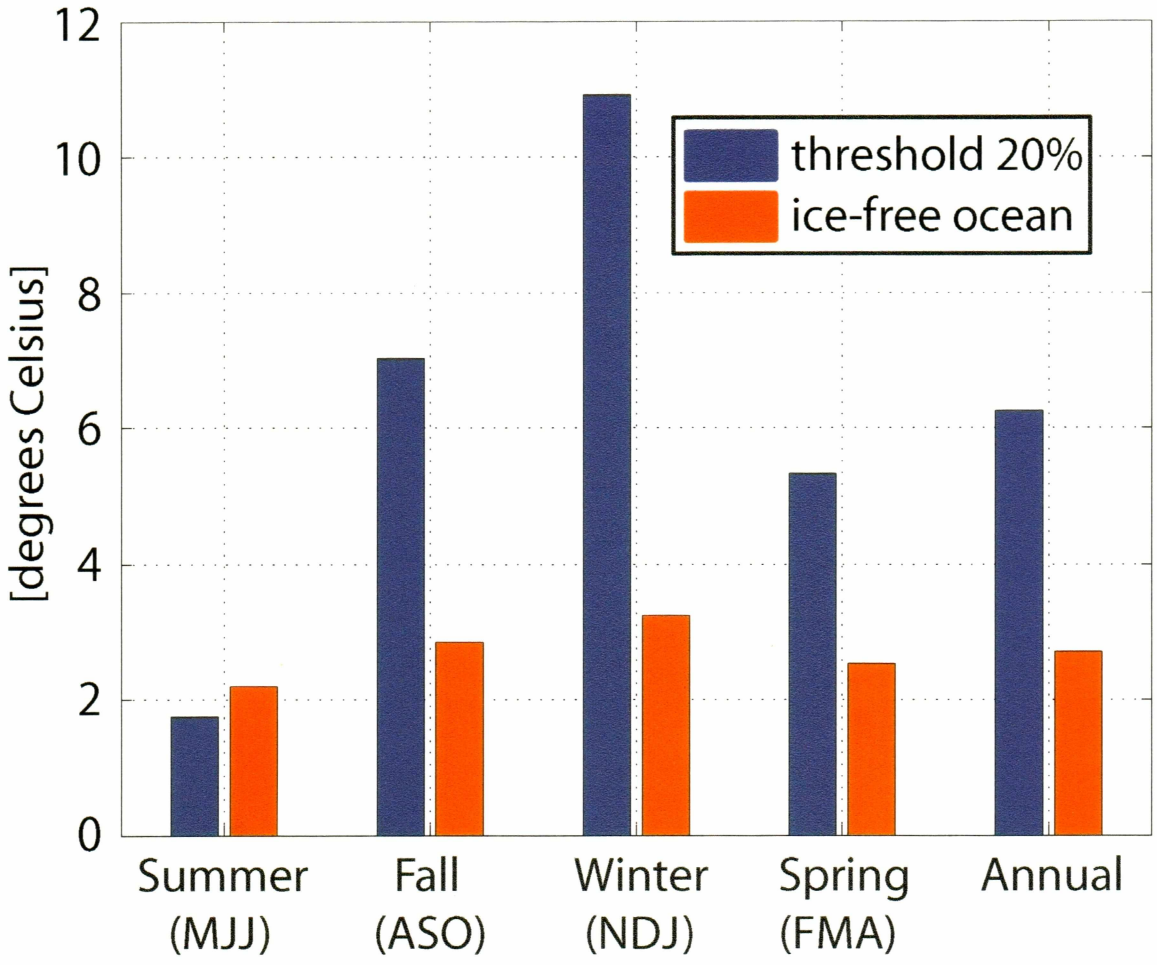


Figure 13. Composite, Seasonal, and 2090's Decadal-Mean Area-Averaged Temperature Anomalies: area-averages over ice-retreat area calculated with a 20% retreat threshold (blue) and over proximate ice-free ocean (red)

## 5. Conclusions

This study has provided an assessment of the local enhancement of warming attributable to sea ice retreat in greenhouse simulations by five global climate models. Although the estimates presented here are lower bounds because the models include horizontal advection, they provide a base upon which more comprehensive evaluations of sea-ice-albedo-temperature feedbacks can build. The main findings are the following:

- Sea ice retreat does not always enhance warming (e.g. summer), but when it does the magnitude of enhancement increases with the threshold used to define retreat because higher thresholds better isolate the warming enhancement signal over ice retreat areas. The uniqueness of the summer result arises from the negative sign of the surface-minus-air temperature differences during summer.

- The models show a wide range of sea ice retreat, resulting in a corresponding range in the enhancement of warming by sea ice retreat. The model with minimal ice retreat not only provides little area for sampling of enhanced warming, but it also shows a weak sea ice signal irrespective of the threshold used to define retreat.

- The enhancement of warming by sea ice retreat is highly seasonal, varying *locally* from essentially zero in the summer to several degrees (°C) in the late autumn and early winter, when it is so strong that it clearly delineates areas of sea ice retreat.

The major challenge to an assessment of this type is to account for the "leakage" of the enhanced warming that results from advection of the additional heat gained over newly ice-free ocean areas. Since some of this heat has already warmed areas that did not

experience sea ice retreat in the model simulations, the sea ice contribution to the warming is underestimated by the methodology used here. Model experiments are planned with CCSM3 with advective fluxes evaluated across the boundaries between sea-ice-retreat areas and other areas, providing a means isolate more clearly the impact of sea ice retreat on the temperature of the Arctic. The results will be placed into a broader context of feedbacks (e.g., Alexeev, 2003).

# References

ACIA, 2004: Impacts of a Warming Climate, Cambridge University Press, Cambridge, U.K., 140 pp.

ACIA, 2005: Arctic Climate Impact Assessment, Cambridge University Press, Cambridge, U.K., 1042 pp.

Alexeev, V. A., 2003: Sensitivity to $CO_2$ doubling of an atmospheric GCM coupled to an oceanic mixed layer: a linear analysis. *Clim. Dyn.,* 20: 775-787.

Boville, B. A., J. T. Kiehl, P. T. Rasch and F. O. Bryan, 2001: Improvements in the NCAR CSM-1 for transient climate simulations. *J. Climate*, 14, 164-179.

Flato, G., G. J. Boer, W. G. Lee, N. A. McFarlane, D. Ramsden, M. C. Reader and A. J. Weaver, 2000: The Canadian Centre for Climate Modeling and Analysis global coupled model and its climate. *Clim. Dyn.*, 16, 451-468.

Gordon, C., C. Cooper, C. A. Senior, H. T. Banks, J. M. Gregory, T. C. Johns, J. F. B. Mitchell and R. A. Wood, 2000: The simulation of SST, sea ice extents and ocean heat transports in a version of the Hadley Centre coupled model without flux adjustments. *Clim. Dyn.*, 16, 147-168.

IPCC, 2000: *Special report on emission scenarios: A special report of Working Group III of the Intergovernmental Panel on Climate Change* (N. J. Nakicenovic and R. Swart, Eds.), Cambridge University Press, Cambridge, U.K., 599 pp.

IPCC, 2001: *Climate Change 2001: The Scientific Basis. Contribution of Working Group 1 to the Third Assessment Report of the Intergovernmental Panel on Climate Change* [Houghton, J.T., Y. Ding, D.J. Griggs, M. Noguer, P.J. van der Linden, X. Dai, K. Maskell, and C.A. Johnson (eds.)]. Cambridge University Press, Cambridge, United Kingdom and New York, NY, USA, 881 pp.

Keeling, C.D. and T.P. Whorf, 2005: Atmospheric $CO_2$ records from sites in the SIO air sampling network. In Trends: A Compendium of Data on Global Change. Carbon Dioxide Information Analysis Center, Oak Ridge National Laboratory, U.S. Department of Energy, Oak Ridge, Tenn., U.S.A.

Knutson, T. R., T. L. Delworth, K. W. Dixon and R. J. Stouffer, 1999: Model assessment of regional surface temperature trends (1949-1997). *J. Geophys. Res.*, 104, 30,981-30,996.

Manabe, S., and R. T. Wetherald, 1975: The effects of doubling the $CO_2$ concentration on the climate of a general circulation model. *J. Atmos. Sci.*, 32, 3–15.

Murray, C., and J. Walsh, 2005: A Model Ensemble Assessment of Arctic Warming by Sea Ice Retreat. *SOLA*, 1, 57-60.

Peterson, T.C., and R.S. Vose, 1997: An Overview of the Global Historical Climatology Network Temperature Database. *Bull. Amer. Meteor. Soc.*, 78, 2837-2849.

Rind, D., R. Healy, C. Parkinson, and D. Martinson, 1995: The Role of Sea Ice in 2 × $CO_2$ Climate Sensitivity. Part 1: The Total Influence of Sea Ice Thickness and Extent. *J. Climate,* 8, 449-463.

Roeckner, E., L. Bengtsson, J. Feichter, J. Lebeveld and H. Rodhe, 1999: Transient climate change simulations with a coupled atmosphere-ocean GCM using the tropospheric sulfur cycle. *J. Climate,* 10, 3004-3012.